Journal of the European Ceramic Society **14** (1994) 1–11

HREM and AEM Studies of Yb_2O_3-Fluxed Silicon Nitride Ceramics with and without CaO Addition

Hans-Joachim Kleebe,* John Bruley & Manfred Rühle

Max-Planck-Institut für Metallforschung, Institut für Werkstoffwissenschaft, Seestraße 92, D-70174 Stuttgart 1, Germany

(Received 16 August 1993; accepted 5 October 1993)

Abstract

The grain-boundary microstructure and interface chemistry of Yb_2O_3/Al_2O_3-fluxed sintered Si_3N_4 materials with and without the addition of CaO has been investigated by means of high-resolution and analytical electron microscopy. Each Si_3N_4 grade examined, exhibited a thin amorphous intergranular layer at both homophase and heterophase boundaries. The presence of calcium within this amorphous layer is confirmed in the CaO-doped materials. Furthermore, no solid solution of CaO within the Si_3N_4-matrix grains could be detected. The observed variability in the grain-boundary film thickness appears to be closely related to changes in the glass composition, in particular to the Ca content. The addition of CaO resulted in a widening of the intergranular film of up to 0·4 nm. Moreover, post-sintering heat-treatment, which induces crystallization of the secondary phase pockets, led to only small changes in the intergranular film thickness of 0·1 nm when compared to the as-sintered specimens, for both CaO-doped and undoped materials.

Die Mikrostruktur der Korngrenzen und die Grenzflächenchemie von Si_3N_4 mit und ohne CaO-Zugaben, das mit Yb_2O_3/Al_2O_3 als Flußmittel gesintert wurde, wurden mit Hilfe von hochauflösender und analytischer Mikroskopie untersucht. Alle untersuchten Si_3N_4-Pulver zeigten eine dünne, amorphe, intergranulare Schicht an Homo- und Heterophasengrenzen. Das Vorhandensein von Kalzium in dieser amorphen Schicht wurde in den CaO-dotierten Materialien bestätigt. Ferner wurde kein CaO-Einbau in die Si_3N_4-Matrix-Körner gefunden. Die beobachteten Unterschiede in der Dicke der Korngrenzfilme scheinen eng verknüpft zu sein mit Änderungen der Glaszusammensetzung, speziell mit dem Ca-Gehalt. Die Zugabe von CaO verursachte eine Zunahme der intergranularen Filmdicke auf bis zu 0·4 nm. Außerdem führte eine Wärmebehandlung im Anschluß an das Sintern, die ein Kristallisieren der Sekundärphasen-Pockets bewirkt, zu geringen Änderungen der intergranularen Filmdicke von 0·1 nm verglichen mit den nur gesinterten Proben, sowohl für CaO-dotierte als auch undotierte Materialien.

Les auteurs ont étudié, par microscopie électronique à transmission à haute résolution et microanalyse, la microstructure des joints de grains et la chimie des interfaces dans des matériaux en Si_3N_4 frittés avec Yb_2O_3/Al_2O_3, avec ou sans addition de CaO. L'examen de chaque nuance de Si_3N_4 a montré la présence d'une fine couche amorphe intergranulaire, qu'il s'agisse d'un joint de grain entre phases identiques ou non. La présence de calcium à l'intérieur de cette couche amorphe a été confirmée dans les matériaux dopés au CaO. De plus, aucune solution solide n'a pu être détectée entre CaO et les grains de la matrice en Si_3N_4. On a observé une variation dans l'épaisseur de film constituant le joint de grain, qui semble liéc étroitement à des modifications de la composition du verre en particulier à la teneur en Ca. L'addition de CAO conduit à un élargissement du film intergranulaire jusqu'à atteindre 0·4 nm. De plus, le traitement thermique après frittage, qui induit la cristallisation de poches de phase sécondaire, ne modifie que très peu (0·1 nm) l'épaisseur du film intergranulaire, ainsi que le montre la comparaison avec des échantillons bruts de fittage, dopés ou non au CaO.

1 Introduction

Grain boundaries, in polycrystalline materials are known to limit important material properties such as mechanical strength, creep resistance, thermal conductivity, critical current density or electrical and optical properties. For sintered Si_3N_4 ceram-

* Present address: Institut für Materialwissenschaft, Lehrstuhl Keramik, Universität Bayreuth, D-95440 Bayreuth, Germany.

ics, a degradation of flexural strength at temperatures ≥1000°C is well known and related to the occurrence of amorphous secondary grain-boundary phases which result during the liquid-phase sintering process.[1–3] The reduction in strength is due to softening of the residual glass phase at such elevated temperatures. Earlier work showed that the creep behaviour of Si_3N_4-based materials is also strongly affected by the presence of amorphous intergranular phases.[4,5] Moreover, Hwang *et al.* reported on the effect of low-melting grain-boundary phases on the superplasticity of Y_2O_3-stabilized ZrO_2.[6]

Deeley and co-workers were first to demonstrate that complete densification of Si_3N_4-powder compacts during pressureless sintering can be achieved only with the aid of sintering additives.[7] This is a result of the high covalent bonding character (approximately 75%) of the Si_3N_4 structure which results in a low self-diffusivity even at 1400°C.[8] Commonly used sintering aids include metal oxides such as MgO and Al_2O_3 and most of the rare-earth oxides.[9–12] The densification can best be described as a liquid-phase sintering process. At elevated temperatures SiO_2, which is always present at the Si_3N_4-particle surfaces, reacts with the metal or rare-earth oxide additives forming a melt. With increasing temperature, the chemical composition of the melt changes to an oxynitride liquid owing to the preferred dissolution of α-Si_3N_4.[13,14] Upon cooling, supersaturation leads to reprecipitation of β-Si_3N_4, either forming small particles in the triple-grain pockets or depositing epitaxially onto pre-existing Si_3N_4 grains.[15] Depending on both the sintering aid composition and processing conditions either amorphous or a combination of crystalline and amorphous secondary phases can form upon cooling.[16] It has been reported that a post-sintering heat-treatment may induce crystallization of the amorphous secondary phase in triple-grain regions.[17–19] Hence, crystallization greatly reduces the volume fraction of residual glass in the material. However, complete crystallization of the glass phase cannot be achieved in these materials, as the thin films between two-grain junctions remain amorphous.[20–22] Recent high-resolution electron microscopy HREM observations have shown that amorphous grain-boundary films with a characteristic film thickness are always present at interfaces in Si_3N_4[23–26] with the only exceptions being 'special' interfaces and low-angle grain boundaries.[27,28] Even hot-isostatically pressed (HIPed) Si_3N_4 materials, processed without the addition of sintering aids, revealed amorphous intergranular films along two-grain junctions with a film width of about 1·0 nm.[29]

In this paper the authors report on investigations of liquid-phase sintered Si_3N_4 materials (SSN), designed to study the influence of sintering additive impurities on the structure and chemistry of the amorphous grain-boundary films. Yb_2O_3/Al_2O_3-fluxed Si_3N_4 was prepared with and without small amounts of CaO addition. CaO was selected owing to the lack of a solid-solution range between CaO and Si_3N_4. The CaO was expected to segregate to triple-grain junctions and grain boundaries, thereby affecting both the local chemistry and the equilibrium thickness of the intergranular phase. A heat-treatment was designed to crystallize the triple-grain pockets and drive the CaO impurity to the grain boundaries and, hence, locally increase the impurity content. High-resolution electron microscopy (HREM) and analytical electron microscopy (AEM) was performed to correlate variations in microstructure and intergranular film thickness with the amorphous grain-boundary film composition.

2 Experimental Procedures

2.1 Materials

Twenty Si_3N_4 samples were processed via liquid-phase sintering at 1780°C for 2 h under 0·1 MPa N_2 pressure. The sintering aid for complete densification consisted of 5 vol.% Yb_2O_3 + 0·43 vol.% Al_2O_3 (for improved sinterability). To ten of the samples was added 0·26 vol.% CaO prior to sintering. After sintering, half of each batch of CaO-doped and undoped materials were heat treated for 12 h at 1250°C under 0·1 MPa N_2 pressure. The material also contains oxygen impurity corresponding to about 4·75 vol% SiO_2.

2.2 TEM foil preparation

TEM foil preparation was performed by standard techniques, which include mechanical grinding and dimpling, ion thinning to perforation, and a light carbon coating to minimize electrostatic charging effects in the electron microscope.

2.3 HREM and AEM investigations

The overall microstructural characterization of each material was performed by means of conventional transmission electron microscopy (CTEM) utilizing a JEOL JEM 2000 FX, fitted with an ultra-thin window Ge energy-dispersed X-ray (EDX) detector. Identification of the crystalline secondary phases formed upon heat treatment was performed by both X-ray diffraction (XRD) and electron diffraction including the convergent beam technique (CBED). For structural analysis of the amorphous grain-boundary films, the HREM imaging technique[30,31] was applied using a JEOL JEM 4000 EX operating at 400 kV, and possess-

ing a point-to-point resolution of 0·17 nm. To quantitatively measure the grain-boundary film thickness of the different materials from HREM images, the 0·66 nm spacings of the $\{10\bar{1}0\}$ planes of β-Si_3N_4 were used as an internal standard. Three to four film-width measurements were taken from each HREM micrograph giving an accuracy of ±0·1 nm.[32]

Grain-boundary film chemistry was determined by spatially resolved EDX and electron energy-loss spectroscopy (EELS) using a Vacuum Generator Microscopes 'HB501' dedicated scanning transmission electron microscope (STEM). The typical spatial resolution routinely available with this instrument is 0·8 nm.

3 Results and Discussion

3.1 As-sintered SSN materials

3.1.1 General microstructure

After sintering, the overall micron-scale microstructure of both the CaO-doped and undoped Si_3N_4 grades are indistinguishable: Small equiaxed, although often faceted Si_3N_4-matrix grains with an average diameter of 1–2 μm are observed adjacent to a small number of larger, more elongated Si_3N_4 particles (15–20% by volume as estimated by SEM and TEM). In contrast to reports in the literature, where Ca addition enhanced grain growth,[33,34] the CaO-doped SSN studied here do not exhibit exaggerated grain growth relative to the undoped material. This difference is attributed to the lower amount of CaO used in this study. The secondary phase material is completely amorphous in both as-sintered SSN materials with and without CaO addition. No crystalline secondary phases are observed. Diffuse dark-field imaging (DDF) displays the distribution of the residual glass; the glass is located within triple-grain regions of the Si_3N_4-matrix grains and between two-grain junctions, as illustrated in Fig. 1.

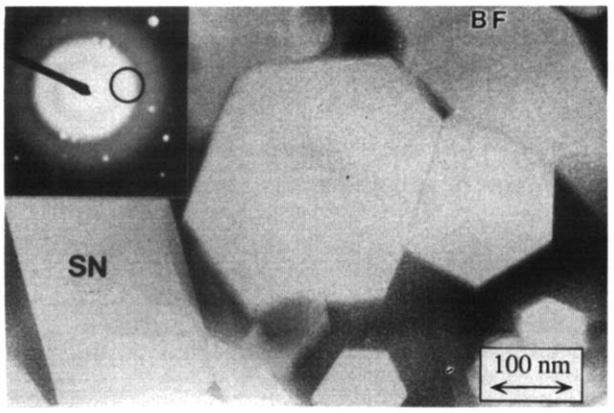

(a)

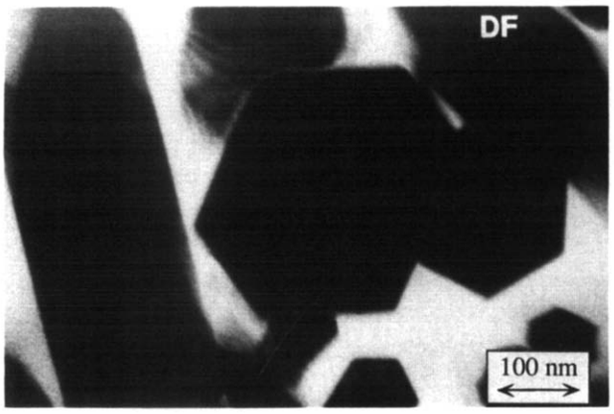

(b)

Fig. 1. (a) Bright field image and (b) diffuse dark field image of as-sintered SSN with 5 vol.% Yb_2O_3 addition revealing the amorphous nature of the secondary phase material observed at both triple-grain junctions of Si_3N_4 matrix grains and along two-grain junctions (homophase boundaries). Note that the as-sintered undoped and CaO-doped materials are indistinguishable using this technique (only additional chemical analysis can distinguish between the two materials).

3.1.2 Grain-boundary films

In contrast to the overall microstructural development, at higher magnification and resolution, one observes marked differences in the grain-boundary film thickness of the doped and undoped as-sintered materials. From measurements of several HREM images, a ubiquitous increase in the grain-boundary film thickness from 1·0 nm to 1·3 nm with CaO addition is ascertained, as listed in Table 1. The accuracy of such measurements is ±0·1 nm. Recent statistical evaluations of these intergranular film widths support the results already reported.[35] An increased film thickness for the CaO-containing sample was further confirmed by using the Fresnel-fringe technique. Figure 2 provides a comparison of grain-boundary film thickness in the Ca-containing and the undoped as-sintered materials. The images were recorded by HREM. In addition, typical spatially resolved EDX and second-difference EELS analyses for these interfacial regions are presented in Fig. 3.

Table 1. Grain-boundary film variability depending on interface chemistry (elements present at the boundary) and post-sintering heat treatment

Material	*Heat treatment*	*Grain-boundary film thickness (Å)*	*Elements in the residual glass*[a]
SSN, 5 Yb + 0·5 Al	As-sintered	10 ± 1	Yb, Si, O, N
SSN, 5 Yb + 0·5 Al + **0·25 CaO**	As-sintered	13 ± 1	Yb, Si, **Ca**, O, N
SSN, 5Yb + 0·5 Al	Annealed	11 ± 1	Yb, Si, O, N
SSN, 5 Yb + 0·5 Al + **0·25 CaO**	Annealed	14 ± 1	Yb, Si, **Ca**, O, N

[a] Al could not be detected owing to overlap with Yb lines.

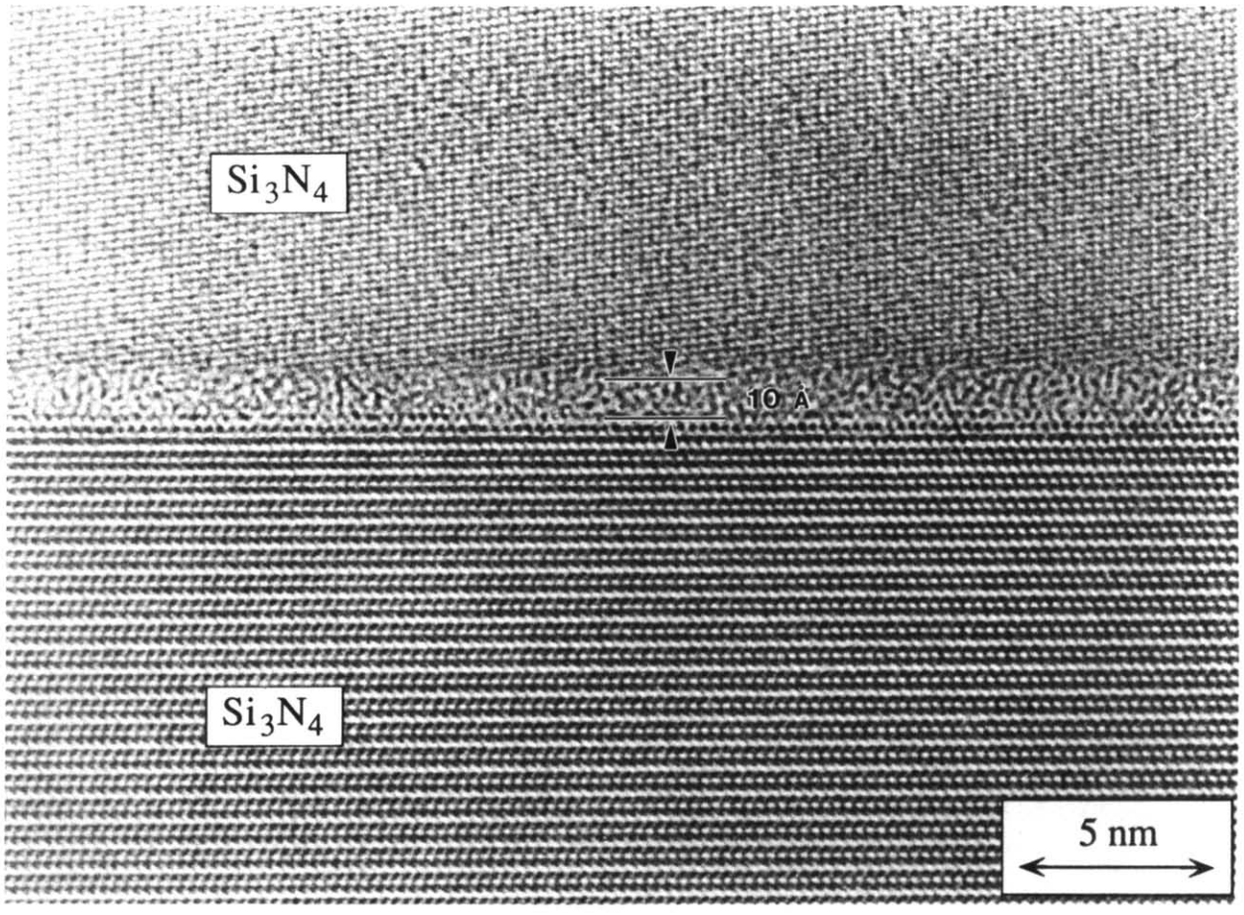

(a)

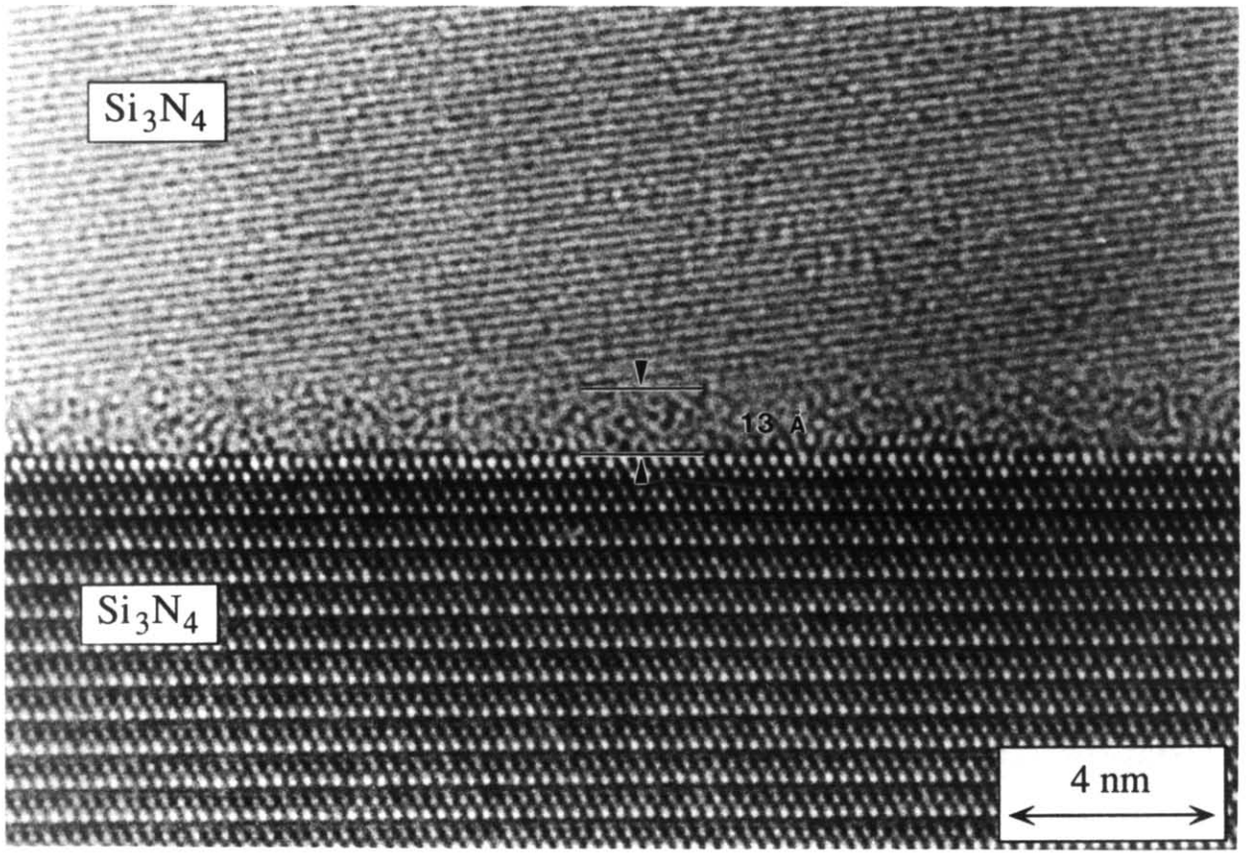

(b)

Fig. 2. HREM images of homophase Si_3N_4 boundaries with an amorphous intergranular film separating the adjacent grains in as-sintered SSN (a) undoped and (b) CaO-doped. Note that the equilibrium film thickness increased from 1·0 nm (undoped) to 1·3 nm (CaO addition).

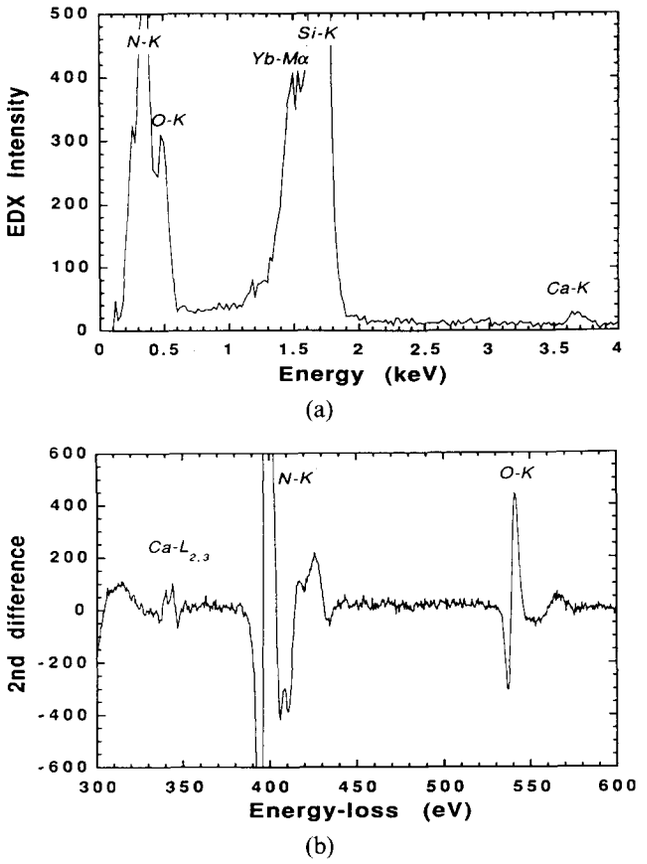

Fig. 3. Typical (a) spatially resolved EDX and (b) second-difference EELS spectra of interfacial regions (homophase boundaries) for the CaO-doped materials. The presence of excess Yb and O (sintering aid) as well as the presence of Ca (doped materials) in the grain-boundary films is ascertained (compare also Fig. 2).

The EDX and EELS spectra show the presence of excess Yb and O at the homophase boundaries as well as the presence of Ca in the doped material.

3.1.3 Analytical electron microscopy

The EDX analysis of a number of amorphous triple-grain regions indicates a homogeneous distribution of Ca in the CaO-doped material. With the fine probe accessible to the STEM, Ca is also found to be present within the intergranular film (see Fig. 3). Apart from Yb, Si, O and N, which were always present in the residual glass, no Ca, which is understood as less than the given detection sensitivity of ≈0·1 at.% Ca, or any other impurities have been detected in the Yb_2O_3-fluxed material (see also Table 1). It should be noted that Al could not be analysed in these materials owing to the overlap with Yb lines. During EDX analysis the overlap of $Al_{K\alpha}$ = 1·478 keV and $Yb_{M\alpha}$ = 1·521 keV strongly limits detectability and during EELS measurements the Al_K = 1560 eV and Yb_{M4} = 1576 eV edges overlap. Al is assumed to be present in the residual glass. Moreover, it is thought that the Al concentration in the glass does not significantly change upon doping but it may significantly increase upon subsequent heat treatment as the crystallisation products found here (see below) do not dissolve much Al. Therefore, a possible influence of Al-concentration on grain boundary chemistry and resulting intergranular film thickness cannot completely be ruled out but cannot be quantified. In both CaO-doped and undoped materials, no reproducibly significant difference in the local chemistry between the grain-boundary film and the triple-grain regions could be detected. Table 2 shows the average grain boundary and triple-junction chemical composition obtained from AEM.

It should be borne in mind that the sensitivity of the EDX technique to detect chemical inhomogeneities in the secondary phase of this system is restricted by electron-beam broadening into neighbouring Si_3N_4 grains (about 5 nm in a 50 nm thick film), and secondary X-ray fluorescence. Spatially resolved EELS is not limited by such effects and thus in some ways offers a superior method for determining localized chemistry. Unfortunately, in this materials system EELS is less sensitive to the *K*-, *L*- and *M*-edges of heavy elements such as Yb, and is adversely effected by the overlap of the N-*K*, Ca-$L_{2,3}$ and the C-*K*-edges (used as a coating). The second-difference technique reduces the influence of edge overlap by enhancing the energy sensitive near-edge structure and significantly reducing the slowly varying background structure. Moreover, recording consecutive spectra from the same region of sample indicates that the grain-boundary films are very sensitive to radiation damage. Techniques designed to minimize the damage include short data acquisition times (<5 s), reduced current density by over-focusing the condenser lens (<0·5 nA/mm^2), and acquisition of both EELS and EDX spectra whilst simultaneously scanning the beam over a 2×3 nm^2 area.

However, it should be emphasized that under the given experimental conditions a reliable quantification of the acquired data is questionable. Figure 4 shows the scatter of data obtained from EDX spectra of the amorphous phases from

Table 2. Average composition ratios of amorphous phases measured using second-difference EELs and EDX spectroscopy

Material	*Ca/O (EELS)*[a]	*Ca/Yb (EDX)*[b]
As-sintered		
Grain boundary	0·006[c]	0·16 ± 0·09
Triple junction	0·008 ± 0·003	0·14 ± 0·04
Annealed		
Grain boundary	0·012 ± 0·004	0·22 ± 0·08
Tip of triple point	0·011 ± 0·004	0·21 ± 0·07

[a] The relative Ca-to-O cross-section ratio for second difference is 37·2.
[b] The relative Ca-to-Yb EDX sensitivity *k* factor is 0·266.
[c] Value based on EDX data.

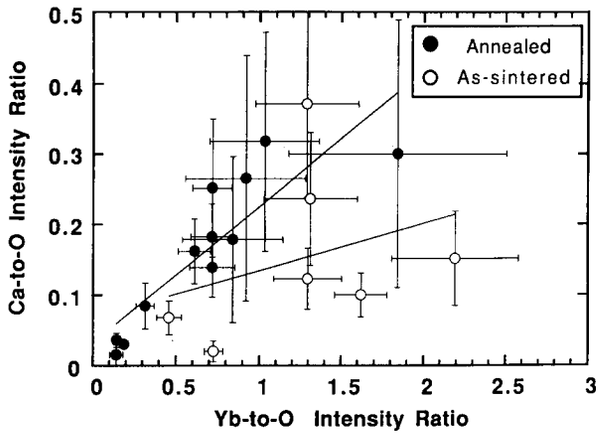

Fig. 4. Spatially resolved EDX measurements of all amorphous secondary phases analysed in the (○) as-sintered and (●) annealed materials. Note the large data scatter which is due to experimental constraints during acquisition, in particular, oxygen loss with acquisition time. However, a clear distinction between the as-sintered and annealed materials can be made.

all materials. The pronounced data scatter of the EDX results is due to the experimental constraints already mentioned, in particular, beam sensitivity of the amorphous material and extended acquisition time during EDX measurements (which leads to an enhanced loss of oxygen with time). Note that despite the large data scatter a clear distinction between as-sintered and annealed materials is found.

The effect the presence of impurity cations has on the grain-boundary film thickness has been the topic of earlier theoretical investigations.[36] According to these considerations changes in the local chemistry and, more importantly, changes in the local charge density and dielectric properties along the interface affect the equilibrium film thickness. With regard to the CaO-doped material, it is thought that the segregation of Ca^{2+} cations to the boundary changes the stoichiometry of the residual glass and hence the surface and space charges along the boundary as well as the dielectric properties of the residual glass. These changes are believed to affect the attractive (van der Waals dispersion force) and the repulsive forces across the homophase boundary (steric force, electrical double layer), thus stabilizing a characteristic equilibrium thickness, which is predicted to be wider compared to the undoped material.[36,37]

The HREM and AEM measurements reported here are consistent with the hypothesis that a change in local (and overall) chemistry, which would modify the properties of the glass film at the interface, alters the intergranular film thickness. It is important to recall that for all Si_3N_4 materials investigated, for a given chemical composition, a *characteristic* grain-boundary film thickness is observed.[23–26,35]

3.2 Heat-treated SSN materials

3.2.1 General microstructure

Post-sintering heat treatment did not change the micron-scale microstructure, described in the previous section, of the doped and undoped heat-treated materials. However, upon post-sintering annealing most of the previously amorphous triple-point regions in both the CaO-doped and the undoped samples became crystalline. Residual glass remains at the tips of each triple junction and also all of the two-grain junctions remain non-crystalline. For the undoped and CaO-fluxed annealed materials different crystalline secondary phases were analysed, as described in detail in Section 3.2.3.

3.2.2 Grain- and phase-boundary films

For characterizing the microstructure of SSN materials containing crystalline secondary phases a distinction between homophase and heterophase boundaries has to be made. In this context, homophase boundaries are present along two-grain junctions of adjacent particles with identical chemistry, such as Si_3N_4/Si_3N_4 boundaries. Heterophase boundaries are between two grains with different chemical composition, such as $Yb_2Si_2O_7/Si_3N_4$ boundaries. It should be noted that the intergranular films at the heterophase boundaries of all Si_3N_4 materials thus far investigated are up to 1–2 nm wider than the homophase boundaries in the same material.[25] This is consistent with the aforementioned theoretical approach[36,37] which predicts lower van der Waals attractive forces for heterophase boundaries, thus resulting in a widening of the film width under the assumption of constant repulsive forces. This is predicted on the expectation that the oxide and oxynitride second phases as well as the glassy films have lower dielectric constants than does Si_3N_4. No systematic study of the heterophase boundary variability was performed, because the triple-grain regions are typically only partly crystalline and, in addition, the secondary phases often reveal relatively rough surface morphologies.

The Si_3N_4–Si_3N_4 boundary-film thickness of the undoped samples is only slightly different before and after heat treatment. An increase in film thickness of 0·1 nm was observed after post-sintering anneal (compare also Table 1). This small deviation is within the experimental error of ±0·1 nm set by the HREM imaging technique.[32] As for the undoped materials, the equilibrium Si_3N_4–Si_3N_4 intergranular film of the CaO-doped materials before and after heat treatment exhibits only a small change in film thickness. Again an increase of 0·1 nm was observed after heat treatment, as

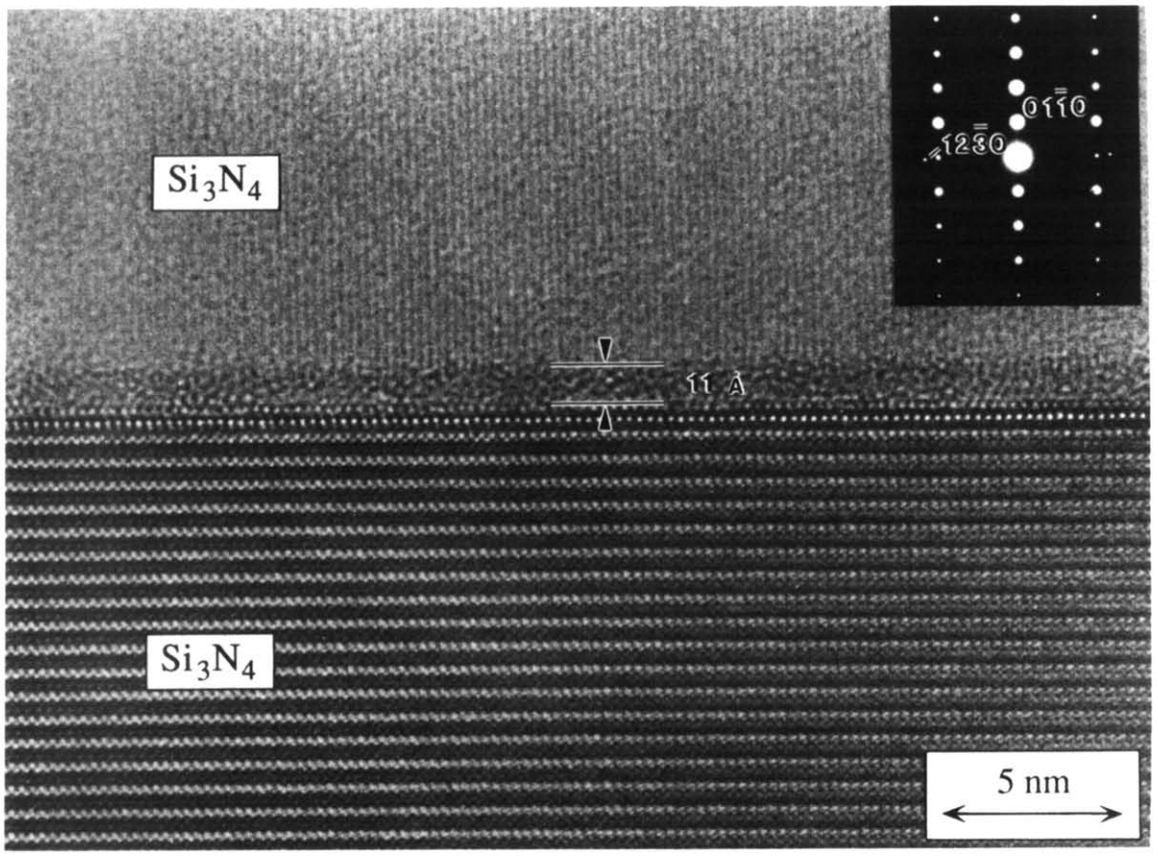

(a)

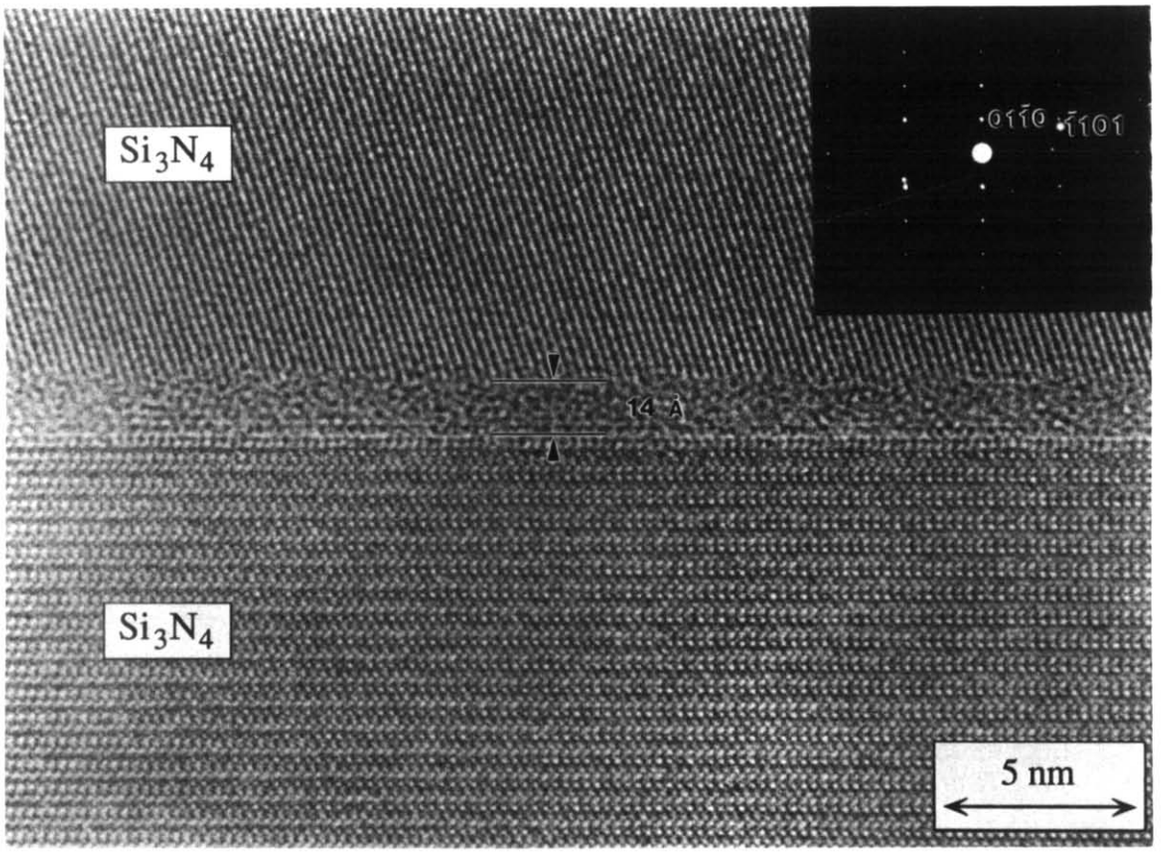

(b)

Fig. 5. HREM images of homophase boundaries from Yb_2O_3-fluxed SSN after post-sintering heat treatment from material (a) without and (b) with CaO addition. The equilibrium film thickness increased from 1·1 nm (undoped) to 1·4 nm (CaO addition). Note that only small changes in grain-boundary film thickness were observed compared to the as-sintered samples (as-sintered = 1·0 nm and 1·3 nm, respectively; see also Fig. 2).

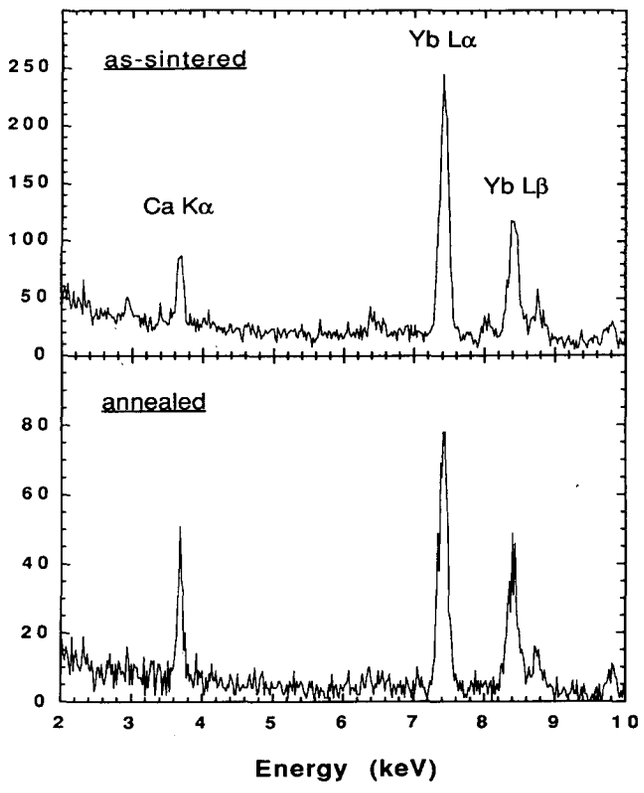

Fig. 6. Spatially resolved EDX analyses of the intergranular film before and after post-sintering anneal which show an increase in Ca content with subsequent heat treatment.

shown in Fig 5. Since both CaO-doped and undoped heat-treated materials showed an identical variation in film thickness, although of rather small increment, it is concluded that crystallization of the secondary phase of SSN prepared with Yb_2O_3/Al_2O_3 slightly changed the interface chemistry. This conclusion is supported by EDX results of the amorphous grain-boundary films in the CaO-doped materials before and after heat treatment, as shown in Fig. 6. An increase in the Ca/Yb ratio of about 40% is observed upon annealing. There appears to be a 50% increase in Ca relative to O and about a 40% increase relative to Yb. With only small changes in composition of the residual glass before and after annealing only a minor change in film thickness is expected. For the undoped materials (before and after post-sintering annealing) the observed small variation in grain-boundary film thickness might be related to small changes in the Al concentration at the interface. Future studies on the Al $L_{2,3}$-edge may be able to confirm this.

3.2.3 Analytical electron microscopy

XRD and electron diffraction identified $Yb_2Si_2O_7$ as the only crystalline secondary phase formed after heat treatment of the undoped material.

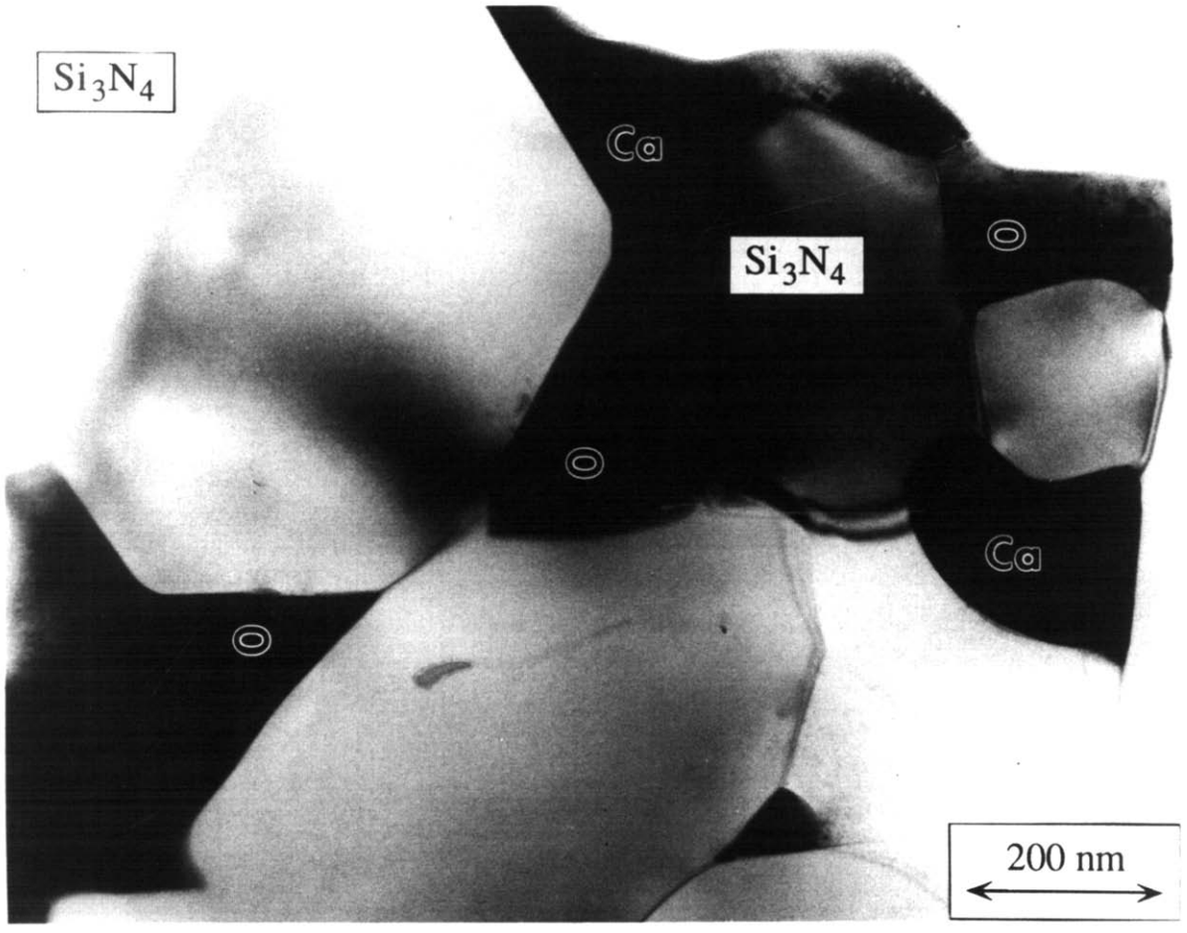

Fig. 7. Bright field image of the CaO-doped Si_3N_4 material after heat treatment. The opposite triple pockets, interconnected by an amorphous intergranular film, are filled with Ca- and N- stabilized apatite (labelled Ca) and pure $Yb_2Si_2O_7$ (labelled O).

However, TEM and STEM investigations of the annealed CaO-containing specimen reveal an unexpected result: apart from the $Yb_2Si_2O_7$ phase, a second crystalline phase is present at triple-grain junctions which contain small amounts of Ca. XRD and electron diffraction identified this phase as $CaYb_9(SiO_4)_6ON$ (Ca- and N-stabilized apatite). Ca is confirmed in the apatite secondary phase by its presence in X-ray emission and second-difference EELS spectra.

At the outset of this work it was anticipated that heat treating the CaO-containing materials would lead to crystallization of the amorphous triple-grain junctions, thereby forcing the CaO impurities to the boundaries, as no solid solution of CaO with the $Yb_2Si_2O_7$ phase is known. This should have led to an increase in impurity content, giving rise to a large increase in grain-boundary film thickness. In practice the formation of an apatite phase is observed. It is known that a higher Ca concentration can stabilize the Yb-apatite structure, but for small amounts no stabilization of this phase was previously observed. It should be noted that XRD measurements of CaO-doped material with CaO additions of less than 1·0 vol.% only revealed the presence of $Yb_2Si_2O_7$ and no Ca-containing phases could be detected.[38]

The distribution of the Ca- and N-stabilized apatite phase seems to be correlated to that of the $Yb_2Si_2O_7$ phase. Observations indicated that a high fraction of 'triple-junction pairs', interconnected by an amorphous film, had the $Yb_2Si_2O_7$ phase on one side and the $CaYb_9(SiO_4)_6ON$ phase on the opposite side of the 'pair', as shown in Fig. 7. One possible explanation for this apparent correlation is that nucleation of the apatite phase is easier in this system. Hence the apatite phase is first to crystallize. With further growth of the Ca-containing phase the residual glass becomes depleted in Ca. The reduction in Ca content in the residual amorphous material results in the formation of the $Yb_2Si_2O_7$ phase in the neighbouring grain pockets, leading to a non-random distribution of crystalline phases. According to this model, segregation and diffusion of Ca cations along the boundary is expected. Segregation of Ca to grain boundaries in addition to low solubility of Ca in Si_3N_4 grains is confirmed by second-difference EELS analysis, as depicted in Fig. 8. It is shown that Ca is present at the intergranular film but no Ca could be detected (below 0·1 at.% detection sensitivity) in the adjacent Si_3N_4 grains (5 nm from interface). Quantitative analysis of Ca concentration profiles (seeking a possible Ca gradient) along the interface layer connecting a $CaYb_9(SiO_4)_6ON$ crystal to a $Yb_2Si_2O_7$ crystal are given in Fig. 9(a) and (b). It should be noted that the EDX data, and in particular the EELS results, do not support the anticipated Ca gradient along the interface layer which connects two crystalline secondary phases. Under the assumption that crystallization of the secondary phase occurs at elevated temperatures rather than upon cooling, it is thought that diffusion

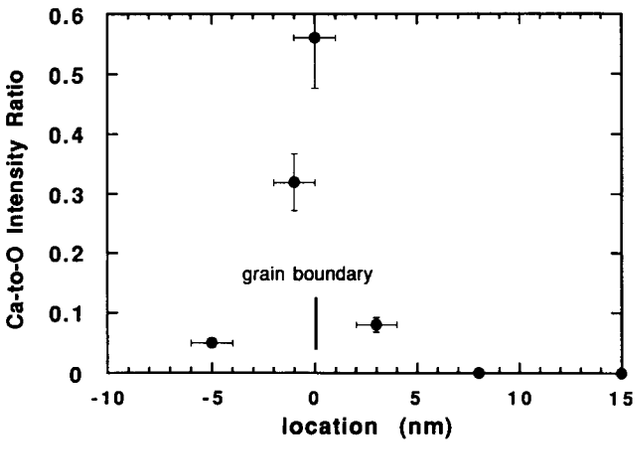

Fig. 8. Spatially resolved second-difference EELS analysis which reveals Ca segregation to the boundary (CaO-doped, as-sintered SSN). Note that no Ca could be detected in the adjacent Si_3N_4 grains.

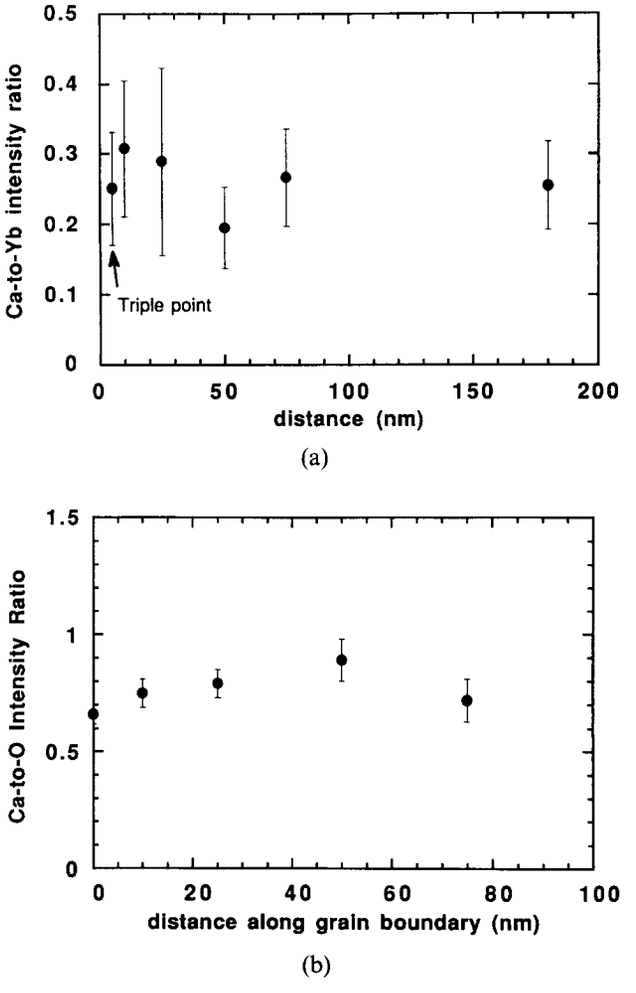

Fig. 9. Spatially resolved AEM studies (a) EDX and (b) second-difference EELS data acquired along the interface (CaO-doped, heat-treated SSN). Note that no chemical gradient was observed.

along interfaces is fast enough, even at moderate sintering or annealing temperatures, to allow for a complete chemical homogenization of the residual glass. Therefore, no composition gradient was detected along the amorphous grain-boundary films.

The observed uniformity of the grain-boundary layer thickness suggests that, if at all present, the chemical gradient should be reasonably shallow. Moreover, with two crystalline secondary phases being observed in the annealed material, one of which contains small amounts of Ca, no great increase in impurity concentration at the interface is to be expected. This explains the near constancy of the grain-boundary film thickness in the as-sintered and annealed materials for the CaO-fluxed specimens (see Table 1). As in the as-sintered material, there is no evidence from the EDS and EELS results to suggest any gross difference (≥1 at.%) in the composition of the amorphous material in the triple points or at grain boundaries. Yb, Si, O and N are detected within the residual glass before and after annealing. In addition, Ca was detected within the amorphous grain-boundary films for both as-sintered and annealed materials.

4 Conclusions

The results indicate that a high concentration of impurity cations, commonly present in the Si_3N_4 starting powders, can segregate to the interfaces and thereby change both interface chemistry and interface structure, which alters the grain-boundary film thickness. Moreover, crystallization of secondary phases can modify the chemical composition of the residual glass and therefore has to be considered while correlating mechanical properties to the interface structure and chemistry. It should be emphasized that even small changes in interface chemistry such as from the addition of CaO affect the intergranular film thickness; however, it is thought that the resulting material properties (high-temperature fracture strength and creep resistance) are mainly governed by interface chemistry and are only less sensitive to the observed film thickness variations. Thus, grain-boundary film thickness is understood as a 'fingerprint' of the interface chemistry and structure, characteristic for each material.

5 Summary

AEM and HREM studies were performed to investigate the dependance of grain-boundary film thickness on interface chemistry in Si_3N_4-based ceramics. In particular the influence of low impurity content was analysed by deliberately adding CaO to the system. Yb_2O_3/Al_2O_3-fluxed SSN with and without the addition of 0·25 vol.% CaO were investigated. After sintering the overall micro-structure of the doped and undoped materials were indistinguishable. All materials showed a characteristic film thickness depending on grain-boundary film chemistry. The CaO-containing materials showed an increase in amorphous grain-boundary film width of 0·3 nm compared to the undoped samples, independent of post-sintering annealing. Subsequent heat treatment induced crystallization of most triple-grain junctions. In the undoped specimen $Yb_2Si_2O_7$ was observed as the only crystalline secondary phase. CaO addition led to the formation of two different crystal-line phases: the $Yb_2Si_2O_7$ phase and a Ca- and N-stabilized apatite phase $CaYb_9(SiO_4)_6ON$. An increase of 0·1 nm of the intergranular film thickness was observed for both doped and undoped materials after post-sintering anneal.

Acknowledgements

The authors are indebted to E. Hampp and M. J. Hoffmann for valuable discussions and for providing the Si_3N_4 materials. Moreover, the authors would like to thank the BMFT for support under the contract number NTS 0230/0.

References

1. Lange, F. F., Fabrication and properties of dense polyphase silicon nitride. *Am. Ceram. Soc. Bull.*, **62**(12) (1983) 1369–74.
2. Sanders, W. A. & Mieskowski, D. M., Strength and microstructure of sintered Si_3N_4 with rare-earth-oxide additions. *J. Am. Ceram. Soc.*, **64**(2) (1985) 304–9.
3. Hirosaki, N., Okada, A. & Matoba, K., Sintering of Si_3N_4 with the addition of rare-earth oxides. *J. Am. Ceram. Soc.*, **71**(3) (1988) C-144–C-147.
4. Tsai, R. L. & Raj, R., The role of grain-boundary sliding in fracture of hot-pressed Si_3N_4 at high temperatures. *J. Am. Ceram. Soc.*, **63**(9–10) (1980) 513–17.
5. Raj, R., Creep in polycrystalline aggregates by matter transport through a liquid phase. *J. Geophys. Rev. B*, **87**(7) (1982) 4731–9.
6. Hwang, C. J. & Chen, I-Wei, Effect of a liquid phase on superplasticity of 2-mol%-Y_2O_3-stabilized tetragonal zirconia polycrystals. *J. Am. Ceram. Soc.*, **73**(6) (1990) 1626–32.
7. Deeley, G., Herbert, J. M. & Moore, N. C., Dense silicon nitride. *Powder Met.*, **8** (1961) 145–51.
8. Kijima, K. & Shirasaki, S., Nitrogen self-diffusion in silicon nitride. *J. Chem. Phys.*, **65** (1976) 2668–71.
9. Terwillinger, G. R. & Lange, F. F., Pressureless sintering of Si_3N_4. *J. Mater. Sci.*, **10** (1975) 1169–73.
10. Loehman, R. E. & Rowcliffe, D. J., Sintering of Si_3N_4–Y_2O_3–Al_2O_3. *J. Am. Ceram. Soc.*, **6**(3–4) (1980) 144–8.
11. Negita, K., Effective sintering aids for Si_3N_4 ceramics. *J. Mater. Sci. Lett.*, **4** (1985) 755–8.
12. Cinibulk, M. K., Thomas, G. & Johnson, S. M., Fabrica-

tion and secondary-phase crystallization of rare earth disilicate–silicon nitride ceramics. *J. Am. Ceram. Soc.*, **75**(8) (1992) 2037–43.
13. Greskovich, C. D., Prochazka, S. & Rosolowki, J. H., Sintering behavior of covalently bonded materials. In *Nitrogen Ceramics*, ed. F. L. Riley. Nordhoff, Leyden, 1977, pp. 351–7.
14. Lange, F. F., Fabrication and properties of dense polyphase silicon nitride. *Am. Ceram. Soc. Bull.*, **62**(12) (1983) 1369–74.
15. Vetrano, J. S., Kleebe, H.-J., Hampp, E., Hoffmann, M. J. & Cannon, R. M., Epitaxial deposition of silicon nitride during post-sintering heat treatment. *J. Mater. Sci. Lett.*, **11** (1992) 1249–52.
16. Tsuge, A., Nishida, K. & Komatsu, M., Effect of crystallizing the grain-boundary glass phase on the high-temperature strength of hot-pressed Si_3N_4 containing Y_2O_3. *J. Am. Ceram. Soc.*, **58**(7–8) (1975) 323–6.
17. Pierce, L. A., Mieskowski, D. M. & Sanders, W. A., Effect of grain-boundary crystallization on the high-temperature strength of silicon nitride. *J. Mater. Sci.*, **21** (1986) 1345–8.
18. Bonnell, D. A., Tien, T. Y. & Rühle, M., Controlled crystallization of the amorphous phase in silicon nitride ceramics. *J. Am. Ceram. Soc.*, **70**(7) (1987) 460–5.
19. Cinibulk, M. K., Thomas, G. & Johnson, S. M., Grain-boundary-phase crystallization and strength of silicon nitride sintered with a YSiAlON glass. *J. Am. Ceram. Soc.*, **73**(6) (1990) 1606–12.
20. Raj, R. & Lange, F. F., Crystallization of small quantities of glass (or a liquid) segregated in grain boundaries. *Acta Met.*, **29** (1981) 1993–2000.
21. Clarke, D. R. & Thomas, G., Grain boundary phases in MgO fluxed silicon nitride. *J. Am. Ceram. Soc.*, **60**(11–12) (1977) 491–5.
22. Clarke, D. R. & Thomas, G., Microstructure of Y_2O_3 fluxed hot-pressed silicon nitride. *J. Am. Ceram. Soc.*, **61**(3–4) (1978) 114–18.
23. Kleebe, H.-J., Vetrano, J. S., Bruley, J. & Rühle, M., TEM studies of grain boundary films in Si_3N_4 ceramics. In *Proc. of 49th Annual EMSA Meeting*, 4–9 August, San Jose, CA, USA, 1991, pp. 930–1.
24. Kleebe, H.-J., Cinibulk, M. K. & Rühle, M., TEM characterization of a ceria-fluxed silicon nitride. *J. Mater. Sci. Lett.*, **12** (1993) 70–2.
25. Kleebe, H.-J., Hoffmann, M. J. & Rühle, M., Influence of secondary phase chemistry on grain-boundary film thickness in silicon nitride. *Z. Metallkunde*, **83**(8) (1992) 610–17.
26. Cinibulk, M. K. & Kleebe, H.-J., Effects of oxidation on intergranular phases in silicon nitride ceramics. *J. Mater. Sci.*, (1992) in review.
27. Schmid, H. & Rühle, M., Structure of special grain boundaries in SiAlON ceramics. *J. Mater. Sci.*, **19** (1984) 615–28.
28. Kleebe, H.-J., SiC and Si_3N_4 materials with improved fracture resistance. *J. Eur. Ceram. Soc.*, **10** (1992) 151–9.
29. Tanaka, I., Kleebe, H.-J., Cinibulk, M. K., Bruley, J. & Rühle, M., Amorphous-grain boundary films in SiO_2 containing Si_3N_4 ceramics. *Phil. Mag. A*, (1993) in review.
30. Krivanek, O. L., Shaw, T. M. & Thomas, G., Imaging of thin intergranular phases by high-resolution electron microscopy. *J. Appl. Phys.*, **50** (1979) 4223–7.
31. Clarke, D. R., On the detection of thin intergranular films by electron microscopy. *Ultramicroscopy*, **4** (1979) 33–44.
32. Cinibulk, M. K., Kleebe, H.-J. & Rühle, M., Quantitative comparison of TEM techniques for determining amorphous intergranular film thickness. *J. Am. Ceram. Soc.*, **76**(2) (1993) 426–32.
33. Evans, J. R. G. & Moulson, A. J., The effect of impurities on the densification of reaction-bonded silicon nitride. *J. Mater. Sci.*, **18** (1983) 3721–8.
34. Giachello, A. & Martinengo, P. C., Impurities effect on sintering on RBSN. In *Proc. VI. CIMTEC, Ceramic Powder, Preparation, Consolidation and Sintering*, ed. A. Giachello. Elsevier, Amsterdam, 1983, 899–907.
35. Kleebe, H.-J., Cinibulk, M. K. & Rühle, M., Statistical analysis of the intergranular film thickness in silicon nitride ceramics. *J. Am. Ceram. Soc.*, **76** (1993) 426–32.
36. Clarke, D. R., On the equilibrium thickness of intergranular glass phases in ceramic materials. *J. Am. Ceram. Soc.*, **70**(1) (1987) 15–22.
37. Clarke, D. R., Shaw, T. M., Philipse, A. P. & Horn, R. G., On a possible electrical double layer contribution to the equilibrium thickness of intergranular glass phase in polycrystalline ceramics. *J. Am. Ceram. Soc.*, **76**(5) (1993) 1201–4.
38. Hoffmann, M. J. & Hampp, E. unpublished work.